ELSEVIER

Journal of Nuclear Materials 288 (2001) 43–56

journal of nuclear materials

www.elsevier.nl/locate/jnucmat

Measurement and analysis of fission gas release from BNFL's SBR MOX fuel

R.J. White [a], S.B. Fisher [a,*], P.M.A. Cook [a], R. Stratton [b], C.T. Walker [c], I.D. Palmer [d]

[a] *British Nuclear Fuels plc, Sellafield, Seascale, Cumbria CA20 1PF, UK*
[b] *Nordostschweizerische Kraftwerke, Parkstrasse 23, Baden CH-5401, Switzerland*
[c] *European Commission, Joint Research Centre, Institute for Transuranium Elements, Postfach 2340, D-76125 Karlsruhe, Germany*
[d] *British Nuclear Fuels plc, Springfields, Preston PR4 OXJ, UK*

Received 10 April 2000; accepted 17 October 2000

Abstract

Puncture results are presented for seven SBR MOX fuel rods from the first prototypical commercial irradiation that was carried out in the Beznau-1 PWR. The rod average burn-up ranged from 31.2 to 35.6 MWd/kgHM. Comparison is made with the percentage of gas released from French MOX fuels and UO_2 fuel. The results show that in the burn-up range investigated, SBR MOX fuel and MIMAS MOX fuel perform similarly, releasing up to about 1% of the fission gas inventory. Comparisons with the Halden Criterion show that SBR MOX has the same release threshold as UO_2 and this suggests that the mechanisms of release in the two fuels are similar. This is further supported by calculations made with the ENIGMA fuel performance code. It is concluded that the apparent differences in fission gas release between SBR MOX and UO_2 fuel, at least in the early stages of release, can be explained by the higher temperatures experienced by MOX fuel.

1. Introduction

BNFL has initiated an extensive irradiation testing and development programme to support the production of its Short Binderless Route (SBR) MOX fuel from its Sellafield MOX plants; the MOX Demonstration Facility (MDF) and Sellafield MOX Plant (SMP). The programme covers as-fabricated characterisation, test reactor irradiations, post irradiation examination (PIE) of commercial LWR fuel and fuel performance modelling. Whilst the basic performance of SBR MOX fuel, in which the plutonium is almost completely homogeneously distributed throughout the pellet, will be similar to that of UO_2, there are expected to be some significant differences in fission gas release and pellet clad interaction (PCI), for example. Some of these differences will be associated with the presence of plutonium in the fuel, others may result from the in-reactor operational strategies appropriate for MOX assemblies which lead to higher end-of-life fuel ratings compared with UO_2 fuel. This distinction must be borne in mind when considering the PIE results, particularly for commercially irradiated fuel.

The first prototypic commercial irradiation of SBR MOX fuel took place from 1994 to 1997 in NOK's Beznau-1 PWR. Four assemblies manufactured in MDF were irradiated to an average assembly burn-up of 33 MWd/kgHM. Seven pre-characterised rods from one of the assemblies, M501, have now been examined in detail at the Institute for Transuranium Elements (ITU). The comprehensive PIE included full non-destructive and destructive programmes to yield key information on all aspects of performance. The early results from these examinations have been published elsewhere [1,2]. In this paper a detailed analysis of the fission gas release from SBR MOX is presented and comparison is made with data from French UO_2 and several different French

* Corresponding author. Tel.: +44-19467 23116.
E-mail addresses: stanfisher@onetel.net.uk, stan@fisher94.freeserve.co.uk (S.B. Fisher).

0022-3115/01/$ - see front matter
PII: S0022-3115(00)00591-2

MOX fuels with significantly different plutonium distributions. Moreover, as the Pu disposition is generally considered to be the microstructural parameter with the greatest influence on gas release in these materials, the as-fabricated structures of the different MOX fuels are compared following a brief introduction to fission gas production and the mechanisms of release.

2. Fission gas release

2.1. Generation of fission gases and the possible consequences of release

A fission event in nuclear fuel results in the creation of two or sometimes three fission products, the emission of between two and three additional neutrons, and the release of around 200 MeV. This appears in the form of the kinetic energy of the products and gives them a recoil range of approximately 6 μm in the oxide fuel. The mass numbers of the fission products vary from around 72, including Zn, Ga and Ge, to 166, including Dy, Ho and Er. The fission process produces unequal mass fragments with the yields of the various products exhibiting a double humped curve as a function of mass number with the maxima in the region of the masses of the krypton and xenon fission gas isotopes. The yields of the long-lived and stable krypton isotopes vary between 0.3% and 2% whereas the yields of the stable xenon isotopes reach values of almost 8%. Whether they are retained in the fuel or released to the rod free volume, these gases can pose a significant problem in the operation of nuclear fuel.

At the start of life, fuel rods are normally pre-filled with helium gas. This has a high thermal conductivity and therefore provides good heat transfer between the outer part of the fuel surface and the cladding. In contrast, the fission gases have thermal conductivities around one twentieth of that of helium and therefore any release into the rod free volume results in a deterioration of the gap conductance and a corresponding increase in fuel operating temperatures. Such thermal feedback effects can lead to escalating swelling and/or fission gas release thereby threatening the integrity of the fuel rod and rendering it liable to failure by PCI or overpressure effects.

2.2. Fission gas release mechanisms

Release by Recoil may occur for any fission fragment created within approximately 6 μm of the fuel surface and release by knockout may result from the collision of a recoiling fission fragment with a fission gas atom within this distance from the fuel surface.

By far the largest contribution to gas release in non-defected fuel rods arises from the diffusion of single fission gas atoms through the UO_2 or MOX lattice to free surfaces or grain boundaries. In the course of this process there is a number of inhibitory factors that delay the occurrence of gas release.

Intragranular gas bubbles are often heterogeneously nucleated in the wake of fission fragments [3] and these may collect fission gas atoms and vacancies thereby providing a sink for gas as well as a source of rapid swelling under adverse transient conditions. These sinks tend to be short-lived under steady-state conditions since an irradiation induced re-solution process acts to return the gas to the matrix following collisions with further fission fragments [4]. Under steady-state conditions, however, a dynamic balance exists between creation and destruction and a certain fraction of the gas in the matrix is trapped in bubbles and unable to diffuse to free surfaces or grain boundaries.

Any intragranular bubbles nucleating near grain boundaries may eventually grow and intersect the boundary where through further collection of gas and vacancies they may be established as intergranular bubbles. These, in turn, may develop through coalescence into grain edge tunnels through which gas may eventually be vented to the fuel free surfaces. This process is termed interlinkage and may recur a number of times during low temperature operation as the edge tunnels grow, interlink, vent, and collapse before repeating the cycle over and over again. At higher temperatures it may appear that the fission gas appears to be released almost continuously.

The delay between the start of the irradiation and the onset of measurable gas release is generally referred to as incubation, but the criteria involved are only vaguely defined. For example, the engineering criterion advanced by the Halden Project [5] relates the onset of measurable gas release at any given burn-up to the fuel centre temperature of the operating rod.

Typically, this threshold relates to releases of around 1% but it should be noted that the gas inventory at 10 MWd/kgU, for example, is only a fifth of that at 50 MWd/kgU. The rod pressurisations resulting from 1% release and their effects on the rod integrity will therefore be markedly different. Attempts have been made to treat the incubation process in terms of the attainment of a saturation concentration on the boundaries after which bubble interlinkage [4,6,7] occurs resulting in gas venting. These have been largely successful without recourse to an arbitrary fractional gas release such as that above.

3. The microstructures of MOX fuels

It is clear from the preceding section that the degree of fission gas release and its timing are dependent on the generation rates of gas atoms and vacancies, their

diffusion to boundaries, and on the concentration of sinks for these species in the matrix. Post-incubation, other parameters such as surface diffusion, which are associated with intergranular bubble growth and interlinkage, become important.

It follows that fuel microstructural features that influence these factors and include, for example, grain size, porosity and, in MOX, the number and distribution of Pu-rich inhomogeneities, should also affect fission gas release. Fabrication method and the resultant fuel microstructure are therefore expected to play a key role in performance.

Aside from SBR, the foremost type of MOX fuel currently manufactured commercially is the MIMAS (micronised master mix) fuel as produced at facilities in Dessel (Belgonucleaire), Cadarache (COGEMA) and Bagnols-sur-céze (MELOX – COGEMA). OCOM (Optimised Co-Milling) is a similar, master mix type fuel that was made by Siemens and has been irradiated in reload quantities in a number of German commercial reactors [8].

3.1. Fabrication routes

The MIMAS and SBR MOX fabrication routes have many steps in common. Both routes manufacture pellets using a press and sinter method, with similar sinter temperatures (approx. 1700°C). Stearate lubricants are also added in both processes. The main differences are how the PuO_2 and UO_2 feed powders are mechanically blended.

3.1.1. MIMAS

The basis of the MIMAS route [9] is the master mix or primary blend. PuO_2, UO_2 and sintered scraps are ball milled for up to 5 h to create an homogeneous mixture of MOX powder containing about 30 at.% HM (heavy metal) Pu. The precise Pu concentration in the master mix can vary between 20 at.% and 40 at.% HM. Powder of the desired final enrichment is then obtained by blending (not milling) the master mix with depleted or natural UO_2. This is known as the secondary blend. It is also possible to add green or even sintered scraps at this stage although this is only performed when there is a large amount of scrap material to recycle. There is an important difference at the secondary blend stage between fuel fabricated by MELOX (melange oxide) and the other facilities. In the conventional MIMAS process, developed at Dessel, UO_2 powder converted by the AUC (ammonium uranyl carbonate) route is used in both the primary and secondary blends. In the MELOX process [10], UO_2 converted by the ADU (ammonium di-uranate) route is used.

In addition to fabrication by the MIMAS process, a limited amount of MOX fuel was made by COGEMA at Cadarache using the COCA (cobroyé-Cadarache) process before it was abandoned. This involves direct co-milling of the oxides and produces a fuel with a homogeneous Pu distribution [10].

3.1.2. SBR

The SBR mixes PuO_2, IDR (integrated dry route)-UO_2 and, potentially, sintered scraps in an attritor mill. The feed powders are added in the proportions of the final enrichment and are milled for a limited time, about 30 min. The high sintered density of the IDR powder requires a pore former to be added. The flow of the milled MOX powder is then improved by spheroidising. Fig. 1 shows a schematic illustration of the SBR fabrication process in SMP.

3.2. Plutonium distribution in SBR and MIMAS MOX

Detailed descriptions of the microstructures of the SBR and MIMAS MOX fuels have very recently become generally available [10–15]. From these papers it is clear that many of the microstructural parameters such as porosity distribution, density and grain size are similar in these MOX fuels, as might be expected from the general requirement to limit in-pile densification. Both fuel types have Pu concentrations in the range 2–7 wt.% HM, depending on enrichment, grain sizes of 5–10 μm, and close to stoichiometric composition with about 95% theoretical density. The one area in which there is a significant difference is in the respective plutonium distributions within the fuel matrix.

Fig. 2 compares electron probe microanalysis (EPMA) Pu distribution maps of the two MIMAS variants [12] with a corresponding image for typical SBR fuel [13–15]. The AUC based product, Fig. 2(a), has the classic duplex structure of about 25 vol% Pu agglomerates in a UO_2/PuO_2 lattice whilst the ADU product, Fig. 2(b), has three different phases: the UO_2 rich matrix, the Pu rich agglomerates, and a coating phase with intermediate Pu content around the particles of UO_2 powder.

The SBR MOX, Fig. 2(c), is much more homogeneous than either the MIMAS-AUC or the MIMAS-ADU fuels. As can be seen from the X-ray map, areas with Pu contents above the matrix concentration are relatively few.

No corresponding information on the microstructure of COCA fuel is available. However, it has been reported [10] as having an homogeneous Pu distribution.

Table 1 gives the proportions of each phase present in the microstructures shown in Fig. 2 and the fraction of the input plutonium in each phase. Whilst SBR MOX consists of 98–99 vol% true mixed oxide with the nominal composition, the MIMAS fuels are comparatively inhomogeneous in respect of their plutonium distribution. Indeed, in the MIMAS-AUC variant over 60% of the input plutonium is

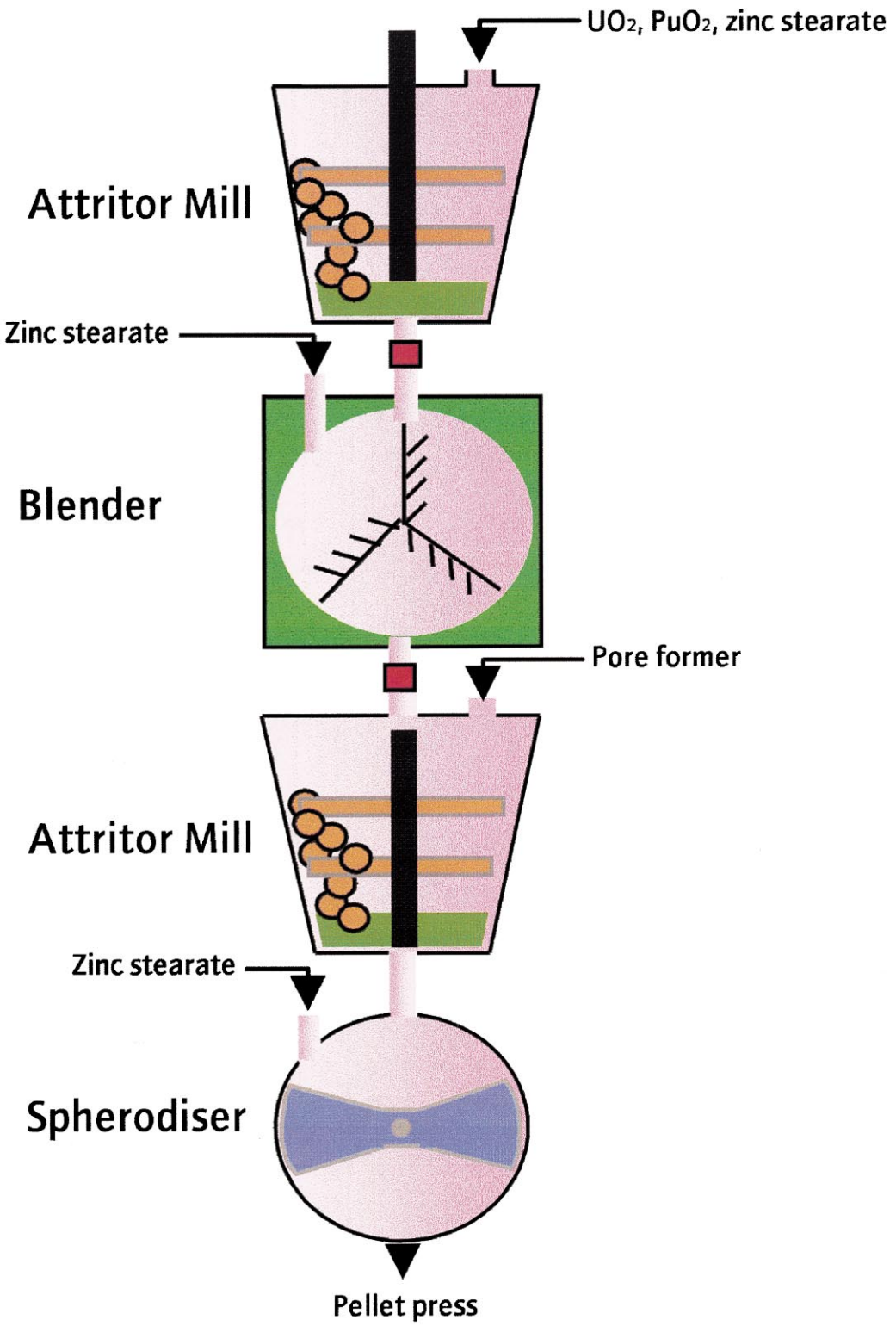

Fig. 1. The Sellafield MOX Plant SBR process.

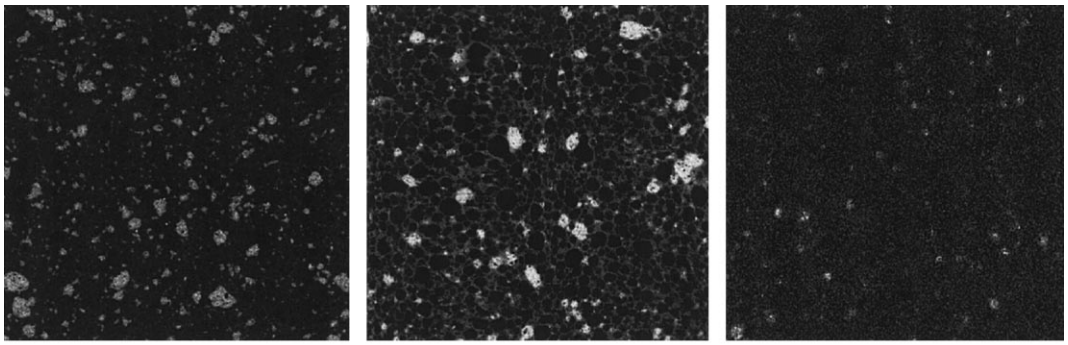

Fig. 2. Plutonium X-ray maps for (a) MIMAS-AUC, (b) MIMAS-ADU and (c) SBR with plutonium contents of 4–5 wt.%. Each map represents an area of approximately 1×1 mm^2. The Pu-rich spots in SBR MOX represent 1–2 vol% of the material and the largest ones are 25–30 μm in diameter (Refs. [12–15]).

Table 1
Area fractions of the phases and distribution of the input plutonium in MIMAS-AUC, MIMAS-ADU and SBR MOX fuel

	Fuel type		
	MIMAS-AUC	MIMAS-ADU	SBR
Area fraction of phases			
Matrix, %	75.4	46.7	98–99
Pu-rich spot, %	24.6	11.1	1–2
Coating around UO_2 particles, %	–	42.2	–
Distribution of input Pu			
Matrix, %	39	15	96
Pu-rich spots, %	61	39	4
Coating around UO_2 particles, %	–	46	–

concentrated in Pu-rich clusters. Not surprisingly the local burn-up distribution in this fuel follows the Pu fissile isotope disposition and the clusters can attain very high burn-ups (>150 MWd/kgHM) [16] with corresponding local accumulations of fission products, including gases. It is now accepted that the fission gas release of this fuel is higher than other more homogeneous fuel [10] and development programmes are in hand to improve this aspect with the current ADU variant. Almost all the irradiation data obtained to date on MIMAS has been from the AUC fuel and it is naturally of interest to compare the fission gas release performance of SBR MOX with that of AUC fuel and, where possible, other French fuels.

4. Experimental

4.1. Characteristics of the M501 fuel and its irradiation history

The design characteristics of the SBR fuel pellets and fuel rods of the M501 assembly are given in Table 2. The pellets used to fill each rod were selected from a single blended lot for each of three plutonium enrichments: low enrichment (L) 2.92 wt.% HM, medium (M) 3.72 wt.% HM, and high (H) 5.54 wt.% HM. The Pu-rich spots occupied 1–2 vol% of the fuel with the largest agglomerates being about 25 μm in size prior to irradiation [15].

The M501 fuel was produced in MDF. The 14×14 assembly of Westinghouse design was irradiated under normal PWR conditions to an average burn-up of 33 MWd/kgHM in the Beznau-1 reactor in Switzerland. The irradiation spanned three operation cycles and lasted 1142 EFPD. The power histories for the seven rods retrieved for PIE at ITU are shown in Fig. 3 [15].

In the first cycle the assembly was located near the periphery of the reactor core and for five of the seven selected rods the average power was only around 15 kW m^{-1}. In the second and third cycles the assembly was positioned closer to the core centre and as a result the linear powers increased to around 20 kW m^{-1} for all the rods. In the second and third cycles the power rating was highest in rod 4567. The average power varied least in rod 4463. In this rod it was around 20 kW m^{-1}

Table 2
Fuel pellet and fuel rod design characteristics for the M501 assembly

Fuel density (%TD)	95
Nominal fuel stack weight (kg)	2.15
Grain size[a](μm)	7.5
Pu content [b](wt.% HM)	2.92, 3.72, 5.54
$^{241}Pu/(^{239}Pu+^{240}Pu+^{241}Pu)$	0.05
$^{240}Pu/(^{239}Pu+^{240}Pu+^{241}Pu)$	0.25
$^{235}U/^{238}U$	0.003
Pu-rich spots[c] (vol%)	1–2
Pu content of Pu-rich spots [c] (wt.%)	25–35
Maximum size of Pu-rich spots [c] (μm)	25–30
Stoichiometry (O/M)	2.00
Pellet diameter (mm)	9.29
He fill gas pressure (bar)	20
Cladding material	Zircaloy 4
Nominal fuel-clad gap width (μm)	100
Free volume (ml)	18

[a] Mean linear intercept.
[b] For three enrichment levels Low, Medium, and High.
[c] Measured by EPMA (see Refs. [14,15]).

throughout the irradiation. In the third cycle the linear power was lowest in rod 4442.

4.2. Rod puncturing

A hollow metal needle was used to puncture each rod in the plenum region allowing its internal pressure to be measured under known temperature conditions. The volume of free gas within each rod was extracted, measured, and retained for isotopic analysis using mass spectrometry. Each rod was then back-filled with helium to determine its internal free volume. The accuracy of the internal pressure measurement was ±1 mbar. The accuracy of the isotopic concentrations measured depends on the volume of gas available. Helium was measured to better than 1%, Xe and Kr to better than 4% and the Xe/Kr ratio to better than 10%. The internal free volume measurements were accurate to better than 5% in all cases.

5. Results

5.1. Gas pressure and rod internal free volume

The results of the rod puncturing are shown in Table 3. In each case there was a reduction in rod free volume of about 35% from the as-fabricated value of around 18 ml to 11.4–12.1 ml which was principally a result of clad creep down with a smaller contribution from fuel swelling. It should be noted that this volume reduction alone would have led to a pressure increase, regardless of any fission gas release. However, the calculated operating pressures, normalised to a coolant temperature of 298°C, would have been less than 65 bar, a satisfactory safety margin with respect to the coolant pressure of 154 bar.

5.2. Gas isotopic composition

The compositions of the gas extracted from the seven rods are given in Table 3. The low measured quantities of nitrogen and oxygen in all the rods confirm their integrity and the helium fill gas concentration shows that very much larger quantities of fission gas could have been accommodated before the internal rod pressure approached the system pressure.

6. Analysis of fission gas release

In order to convert the fission gas volumes in Table 3 into fractional release values the total fission gas generated within the fuel must be calculated. This is done, conventionally, through use of the fission product yields of the long-lived and stable fission gas isotopes listed in Table 4. The yield values given in Table 4 are taken from the OECD's nuclear data PC program, JEF-PC [17].

The calculation of total fission gas generated is more complex for MOX fuel than for UO_2 fuel because of the evolution of the ^{239}Pu and ^{241}Pu fissile isotope concentrations throughout the irradiation and it is worthwhile outlining the various steps involved in the calculation.

6.1. Fission yields

The simple picture represented by the fission yields given in Table 4 is complicated by conversion through neutron capture. Radioactive ^{135}Xe is transformed to the long lived ^{136}Xe by neutron capture making accurate estimates of fission gas yield in this instance dependent on the neutron flux spectrum and therefore the reactor irradiation conditions. Here, the conversion ratio is derived using the reactor physics code CASMO [18] as described later in Section 6.3.

The final mix of fission gases will also show departures from the expected yields because of the transformation of ^{83}Kr to ^{84}Kr and ^{131}Xe to ^{132}Xe by neutron capture. However, these processes do not influence the overall quantity of fission gas generated.

There is a contribution to the long-lived gas inventory from the conversion of ^{133}Xe, which has a 5.25 day half-life, to stable ^{134}Xe by neutron capture. However, the thermal cross-section for this reaction is 195.2 barn [17] which leads to a conversion rate less than 0.1% of the ^{133}Xe production rate.

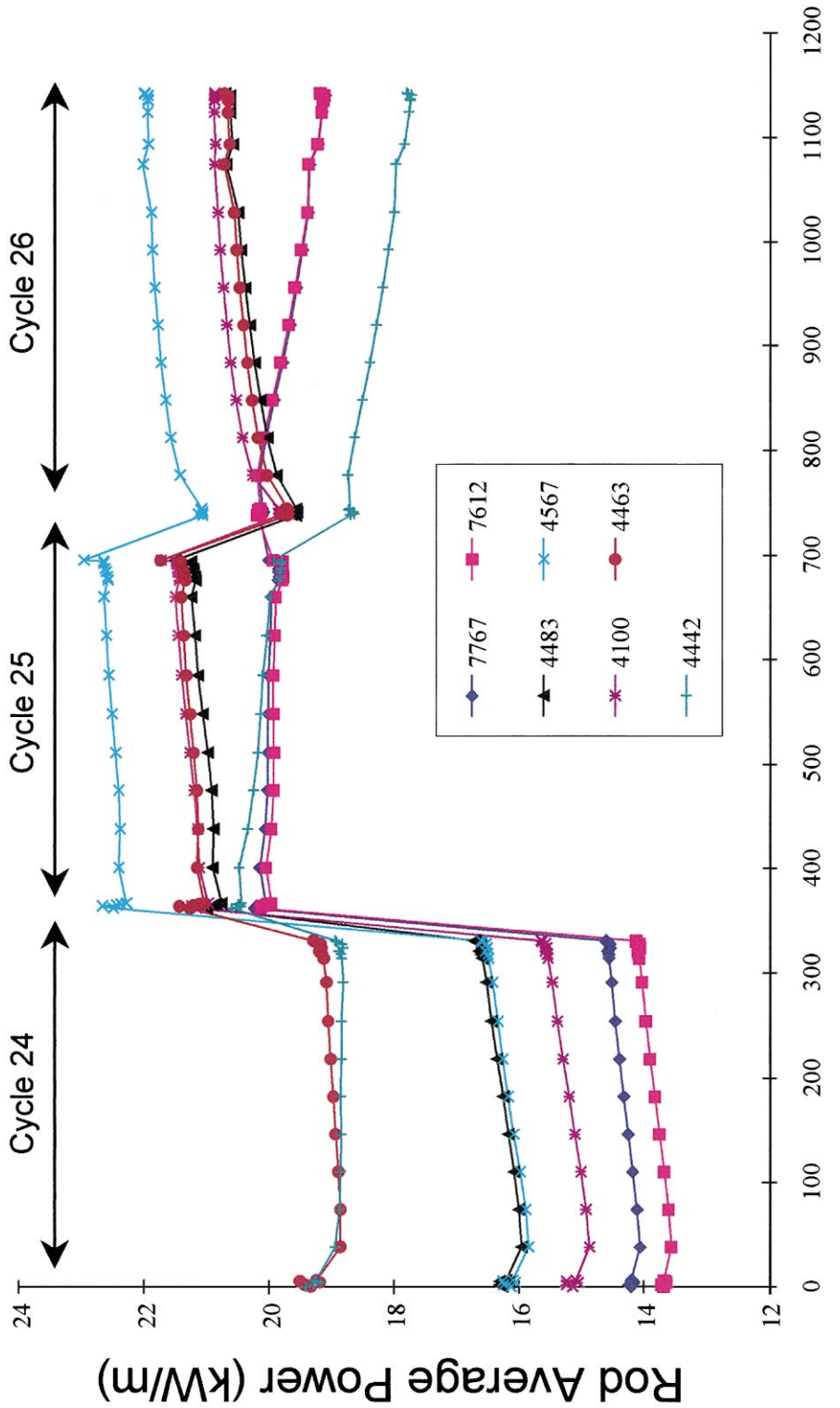

Fig. 3. Calculated rod average power versus dwell time for M501 rods. The first two cycles each corresponded to assembly average burn-ups of roughly 10 MWd/kgHM (Ref. [15]).

Table 3
Puncturing and isotopic analysis results for the gas in the M501 rods[a]

Rod no. (enrichment)	4100 (H)	4463 (H)	4483 (H)	4567 (H)	7612 (M)	7767 (M)	4442 (L)
Burn-up (MWd/kgHM)	33.87	33.71	32.74	35.60	31.17	31.18	32.54
Pressure (bar)	32.58	33.20	33.43	33.99	32.67	32.00	33.13
Rod free volume (ml)	11.50	11.73	11.60	12.13	11.61	11.71	11.40
Total gas volume (ml)	335.43	349.68	347.80	369.59	339.51	335.18	339.10
He	324.76	338.07	338.28	348.02	331.22	327.17	331.08
N_2	0.23	0.20	0.22	0.20	0.33	0.30	0.31
O_2	0.09	0.09	0.09	0.09	0.10	0.10	0.10
Ar	0.23	0.45	0.26	0.67	0.72	0.49	0.48
CO_2	0.45	0.50	0.48	0.50	0.42	0.47	0.50
^{83}Kr	0.09	0.09	0.08	0.18	0.06	0.06	0.06
^{84}Kr	0.17	0.19	0.15	0.37	0.12	0.12	0.12
^{85}Kr	0.04	0.04	0.03	0.08	0.02	0.02	0.03
^{86}Kr	0.25	0.27	0.22	0.54	0.18	0.17	0.17
Total Kr	0.55	0.59	0.48	1.17	0.38	0.37	0.38
^{131}Xe	0.91	0.93	0.78	1.85	0.59	0.58	0.56
^{132}Xe	2.11	2.26	1.84	4.41	1.45	1.44	1.43
^{134}Xe	2.56	2.73	2.27	5.29	1.74	1.72	1.69
^{136}Xe	3.55	3.85	3.10	7.40	2.56	2.53	2.58
Total Xe	9.13	9.77	7.99	18.95	6.34	6.27	6.26
Xe/Kr	16.60	16.56	16.65	16.20	16.68	16.95	16.47

[a] (H) high, (M) medium and (L) low enrichment. The gas pressure, rod free volume and gas volume were measured at STP. The measurements were made in October 1998. The rods were discharged from the reactor in September 1997.

Table 4
Krypton and xenon isotope yields and Xe/Kr ratios from thermal fission of ^{235}U, ^{239}Pu and ^{241}Pu and fast fission of ^{238}U[a]

Fission gas isotope	Yield, atom fraction per fission			
	^{235}U thermal	^{238}U fast	^{239}Pu thermal	^{241}Pu thermal
^{83}Kr	0.0055	0.0040	0.0029	0.0020
^{84}Kr	0.0101	0.0065	0.0047	0.0035
^{85}Kr	0.0029	0.0020	0.0013	0.0009
^{86}Kr	0.0196	0.0130	0.0077	0.0061
Long-lived kryptons	0.0381	0.0255	0.0166	0.0125
^{131}Xe	0.0289	0.0330	0.0387	0.0307
^{132}Xe	0.0427	0.0507	0.0526	0.0408
^{134}Xe	0.0775	0.0754	0.0756	0.0760
^{136}Xe	0.0627	0.0655	0.0694	0.0671
Long-lived xenons	0.2118	0.2246	0.2363	0.2146
Radioactive ^{135}Xe	0.0658	0.0657	0.0723	0.0728
Xe/Kr (minimum)	5.56	8.81	14.23	17.31
Xe/Kr (maximum)	7.29	11.38	18.59	23.18

[a] Yield values are taken from JEF-PC (Ref. [17]). The maximum Xe/Kr ratio assumes that all the radioactive ^{135}Xe created is present; the minimum Xe/Kr ratio assumes that ^{135}Xe is absent.

6.2. Estimation of the through-life fission mix

Under irradiation in a PWR it is expected that the majority of fissions in MOX fuel will arise from thermal fission of the fissile Pu isotopes. However, there will also be a small thermal fission contribution from ^{235}U, and a non-negligible fast fission contribution from ^{238}U. Table 4 shows that these fissions can have significantly different yields for some of the gas isotopes which means that the precise mix of the fission types throughout life

determines both the amount of fission gas produced and its isotopic content.

The physics code CASMO [18] has been used to obtain an accurate through-life fission breakdown for one of the rods, 4567, and this has been assumed to be representative of the others. The through-life fission mix for rod 4567 is calculated by the code to be: 65.8% ^{239}Pu, 23.2% ^{241}Pu and 2.2% ^{235}U. Fissions in these isotopes are assumed to be predominantly at thermal energies. The remaining fissions come mainly from ^{238}U, but with minor contributions from ^{240}Pu and also from other Pu, Am and Cm isotopes. For simplicity, the whole of the remaining 8.8% is assumed to be fast fissions in ^{238}U. The average through-life fission contribution from ^{241}Pu as a percentage of total Pu fissions is therefore 26% compared to its starting value of about 8.8%, corresponding to its initial composition of 6.7% fissile Pu. This increase is a consequence, principally, of progressive ^{239}Pu burn-up and neutron capture in ^{240}Pu.

With the above information it is possible to evaluate the individual weighted fission yields from the data in Table 4. The resulting figures are tabulated in Table 5.

6.3. The ^{135}Xe conversion rate and the total fission gas yield

The CASMO code has also been used to determine the ^{135}Xe to ^{136}Xe conversion ratio, α. In the same way as previously a full analysis has been performed for rod 4567 and assumed representative of all rods. The code calculates the lifetime average thermal flux as 1.5×10^{13} n cm^{-2} s^{-1} and the energy-weighted ^{135}Xe capture cross-section as 1.06×10^{6} barn. The product of these is 1.6×10^{-5} compared with the decay constant of 2.12×10^{-5}, implying a value for the conversion ratio, α, of 43%.

Table 5
Lifetime average estimated fission gas yields for the M501 rods[a]

Fission gas isotope	Yield
^{83}Kr	0.0028
^{84}Kr	0.0047
^{85}Kr	0.0013
^{86}Kr	0.0081
Long-lived kryptons	0.0169
^{131}Xe	0.0361
^{132}Xe	0.0495
^{134}Xe	0.0757
^{136}Xe	0.0684
Long-lived xenons	0.2297
Radioactive ^{135}Xe	0.0717
Xe/Kr (minimum)	13.59
Xe/Kr (maximum)	17.83

[a] The maximum Xe/Kr ratio assumes that all the radioactive ^{135}Xe created is present; the minimum Xe/Kr ratio assumes that ^{135}Xe is absent.

Table 6
Fractional fission gas release from the M501 rods[a]

Rod no.	Burn-up (MWd/kgHM)	Fission gas release (%)
4100 (H)	33.87	0.56
4463 (H)	33.71	0.60
4483 (H)	32.74	0.50
4567 (H)	35.60	1.10
7612 (M)	31.17	0.42
7767 (M)	31.18	0.41
4442 (L)	32.54	0.40

[a] (H) high, (M) medium and (L) low enrichment.

It is interesting to calculate the value of the Xe/Kr ratio that follows from this figure

$$\mathrm{Xe/Kr} = (0.2297 + 0.0717\alpha)/0.0169 = 15.42. \quad (1)$$

This value falls within the 10% range of uncertainty of the measured value for rod 4567 of 16.2.

The above value for α can now be used to derive the total fission gas generation for the M501 rods and, in conjunction with the measured gas volumes, the corresponding fractional gas releases.

6.4. Fission gas release fractions

The average energies from the fission events in ^{239}Pu, ^{241}Pu, ^{235}U, ^{238}U (fast) are 204.5, 206.3, 198.3 and 199.7 MeV, respectively. With the calculated fission distribution the average energy released per fission in the M501 rods is therefore 204.4 MeV $= 3.275 \times 10^{-11}$ J.

Since 1 MWd is equivalent to 8.64×10^{10} J, the fission gas generation for 1 MWd is equivalent to $(8.64 \times 10^{10} \times 0.277)/3.275 \times 10^{-11} = 7.31 \times 10^{20}$ gas atoms. 1 mole of gas at STP occupies 22.4 l, so the gas generation per MWd is given by,

$$2.24 \times 10^{4} \times 7.31 \times 10^{20}/6.022 \times 10^{23} = 27.19 \text{ ml}.$$

From the burn-ups and the weights of fuel in the individual rods the fractional fission gas releases may be calculated and these are tabulated in Table 6.

6.5. Individual isotopic yields

The determination of the total fission gas yield allows the fractional values for each individual isotope to be computed and these may be compared with the measured rod averages to assess the validity of the overall approach to the calculation of fission gas release.

In Fig. 4 the rod average of the measured volume for each individual isotope expressed as a percentage of the total fission gas volume (all from Table 3), is plotted against the corresponding calculated isotopic yield,

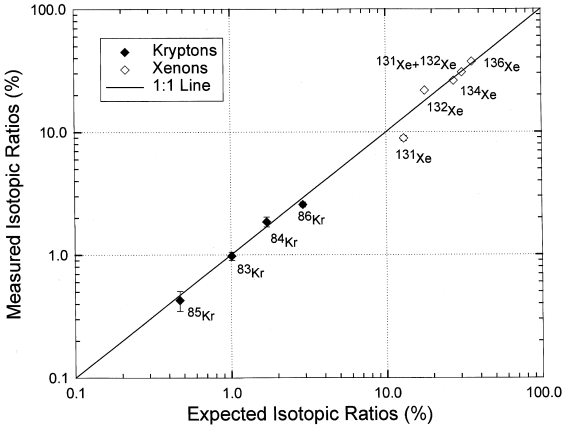

Fig. 4. Rod average measured volume of each individual isotope expressed as a percentage of the total fission gas volume (from Table 3) versus the corresponding calculated isotopic yield (from Table 5) expressed as a percentage of the total yield of 0.277. Error bars for the Xe isotopes are within the symbols. The discrepancies for the ^{131}Xe and ^{132}Xe isotopes arise from neutron capture. The sum of the measured rod average volumes is in good agreement with the calculated value.

expressed as a percentage of the calculated total yield of 0.277 (all from Table 5). The agreement for most isotopes is very good although the points for the ^{131}Xe and ^{132}Xe isotopes do depart significantly from the straight line. Here it is known that neutron capture during irradiation effects a conversion from ^{131}Xe to ^{132}Xe (Section 6.1) and for these two isotopes the sum of the rod averages of their measured percentage volumes is in good agreement with the corresponding sum of the calculated percentage isotopic yields (see Fig. 4).

7. Discussion

7.1. M501 fission gas release fractions

The fission gas release fractions for the M501 rods are in the range in which the mechanisms of release can clearly be associated with changes in the intergranular microstructure. That is, the releases arise from diffusion to the grain boundaries followed by porosity interlinkage on the grain boundaries rather than diffusional release from free external surfaces or direct mechanisms such as recoil and knockout. The spread in values from 0.4% to 1.1% is probably associated with differences in irradiation within the M501 assembly; that is, with the ratings and burn-ups.

7.2. Comparison with other MOX

The releases as a function of burn-up are shown in Fig. 5 along with French data from three-cycle MIMAS-

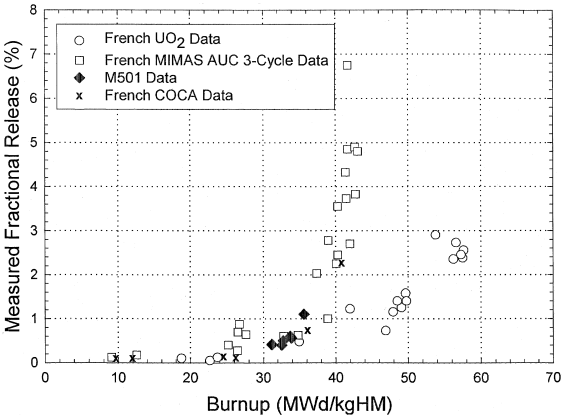

Fig. 5. Measured fractional fission gas releases from MIMAS-AUC and COCA MOX rods compared with those from SBR MOX rods irradiated in the M501 programme. Data from French UO_2 irradiations are also included for the purposes of comparison.

AUC MOX, COCA MOX and UO_2 [10,19]. To simplify the comparison the later French data on four-cycle MIMAS-AUC irradiated to burn-ups of 52–53 MWd/kgHM [20,21] have not been included in the plot. The burn-ups of the M501 rods are not sufficient to determine whether SBR fuel exhibits the steep rise in release with exposure shown by the MIMAS-AUC in the range at 37–40 MWd/kgHM, which is due to the scatter in the power histories of these rods. However, it is clear that fission gas release on SBR fuel does begin at a lower burn-up than in UO_2 fuel.

In Fig. 5 there are some French rods with a similar burn-up to the M501, 32–37 MWd/kgHM, for which the ratings have been reported [19]. Fig. 6 compares the gas

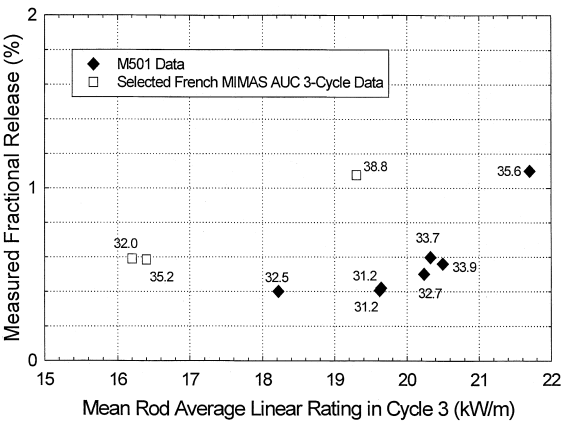

Fig. 6. Dependence of the fission gas release fraction on the rod average linear rating during the third cycle of irradiation for the M501 rods and selected French MOX rods of comparable burn-ups. The individual burn-ups in MWd/kgHM are shown as annotations to the figure.

release data for these rods with the M501 data as a function of the mean rod average rating in the third, and final, cycle. It is seen that the percentage of fission gas released from SBR MOX at 18–22 kW m^{-1} is similar to that obtained from MIMAS-AUC at 16–19 kW m^{-1}. However, since the data are all at around the same burn-up, these particular French rods must have had correspondingly higher ratings at some time during the first two cycles, and this may have contributed significantly to the overall gas release.

Fig. 7 compares the fission gas release of the two homogeneous fuels, SBR and COCA, with the MIMAS-ADU. At current levels of exposure these fuels do seem to be very similar in performance with respect to gas release, however at this stage there is very little difference from the more inhomogeneous MIMAS-AUC.

7.3. Comparison with UO_2 and the Halden Criterion

In order to explore the reasons for the observed early release of fission gas in the SBR MOX compared with UO_2 it is instructive to examine this release in relation to the Halden Criterion [5]. Estimates of the peak centre temperatures of the M501 rods during their final cycle can be made from the operating histories using the ENIGMA fuel modelling code which takes into account the generally lower thermal conductivity of mixed oxide fuels [22]. Table 7 lists the peak calculated temperatures and measured fission gas releases and compares them with the temperatures calculated from the Halden Project Fission Gas Release Threshold [5], which is given by the following equation:

$$B_{\mathrm{rel}}\ (\mathrm{MWd/kgHM}) = 0.00567\mathrm{e}^{9800/T_{\mathrm{c}}} \tag{2}$$

where B_{rel} is the rod average burn-up for 1% gas release and T_{c} is the peak centre temperature in °C. It can be seen that the releases are in proportion to the difference between the calculated peak temperature and the expected temperature for release calculated from the Halden Criterion. This is further emphasised in Fig. 8 where it can be seen that the 1% gas release line is

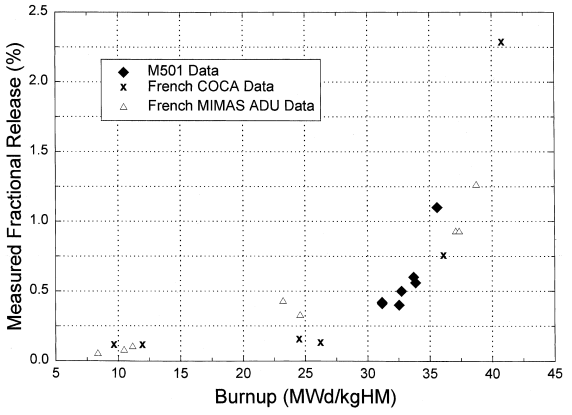

Fig. 7. Measured fractional fission gas releases for French COCA and MIMAS-ADU fuels as a function of burn-up compared with the M501 data.

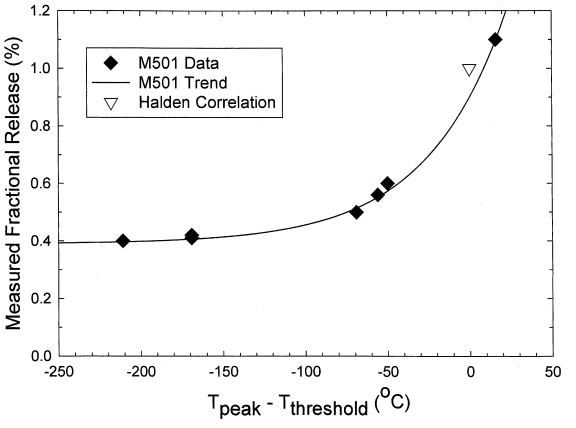

Fig. 8. Measured fractional fission gas release as a function of the difference between the ENIGMA calculated peak centre temperature and the corresponding Halden Fission Gas Release Criterion. Note that the Halden Criterion is the fuel centre temperature for 1% fission gas release from UO_2.

Table 7
Comparison of peak temperatures in third cycle with Halden Criterion[a]

Rod no.	Burn-up (MWd/kgHM)	Gas release (%)	Peak temp. (°C)[b]	Halden temp. (°C)	ΔT (°C)
4100 (H)	33.87	0.56	1071	1127	−56
4463 (H)	33.71	0.60	1077	1127	−50
4483 (H)	32.74	0.50	1062	1131	−69
4567 (H)	35.60	1.10	1136	1120	+16
7612 (M)	31.17	0.42	969	1138	−169
7767 (M)	31.18	0.41	969	1138	−169
4442 (L)	32.54	0.40	921	1132	−211

[a] (H) high, (M) medium and (L) enrichment.
[b] Predicted with the ENIGMA computer code (Ref. [22]).

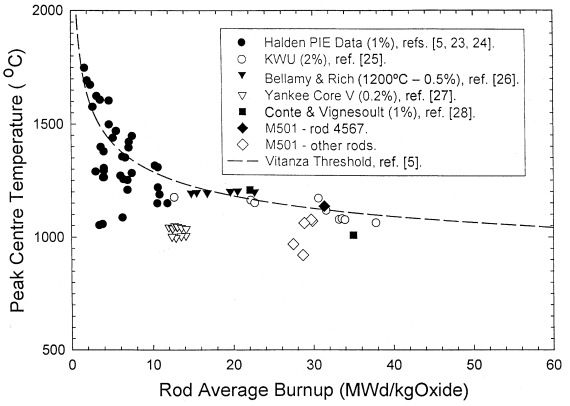

Fig. 9. Comparison of the calculated peak fuel centre temperature in the M501 rods with the Halden empirical fission gas release threshold. The 4567 rod showed just over 1% fission gas release and the point is just above the Halden Threshold while the points for the other rods with below 1% release sit below the line. Note that the line was derived from data for UO_2 fuel and in this figure is presented as a function of the burn-up unit, MWd/kg oxide.

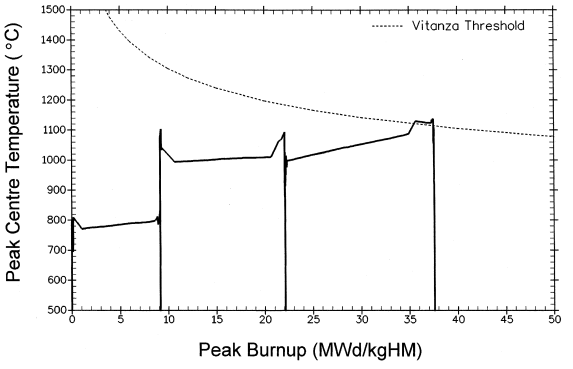

Fig. 10. This plot shows the ENIGMA predictions for the M501 lead rod 4567. The burn-up and temperature shown are the local values at the peak of the axial power profile. For this zone the end-of-life burn-up is predicted to be 37.6 MWd/kgHM and the fission gas release 1.7% consistent with just crossing the Vitanza threshold. For the rod as a whole the predicted burn-up is 35.6 MWd/kgHM and the release 1.0%.

breached for temperatures very close to the expected Halden Criterion predictions. The calculated temperatures are also shown on the standard Halden plot [5,23] in Fig. 9 with the datum point for rod 4567 (>1% release) shown as a closed symbol and the data points for the other rods (<1% release) shown as open symbols, again confirming the conformance with expectations.

This simple analysis goes some way to confirm the similarity of the mechanisms of diffusion and release in the incubation phase in homogeneous MOX and UO_2 and even the comparable values of parameters involved in the process as discussed in Section 3.

7.4. Comparison with ENIGMA predictions

The analysis can be taken a stage further through extended use of the ENIGMA code. If the mechanisms in MOX and UO_2 are indeed the same then this code, which is UO_2-based, should be capable of accurate prediction of the release in rod 4567 if the version which includes the necessary 8% reduction in thermal conductivity is used, as above [22]. Fig. 10 shows the 4567 predictions, in terms of peak zone temperature versus peak zone burn-up, the peak temperature (1136°C in Table 7) being reached at the end-of-life. The corresponding end-of-life peak burn-up is 37.6 MWd/kgHM with a release of 1.7%, figures that translate into whole rod values of 35.6 MWd/kgHM and 1.0% that are very close to those in Table 7, reinforcing the correspondence of SBR MOX with UO_2 fuel.

Fig. 10 also illustrates the importance of the third cycle power level in determining the onset of 1% release and strongly supports the use of the Halden Criterion for simple MOX assessment studies.

7.5. Effects of MOX thermal conductivity and enhanced third cycle rating

The fact that SBR MOX release data, at least in the early stages, can be reproduced using ENIGMA with an appropriate reduction in conductivity suggests that the observed differences from UO_2 are simply attributable to higher fuel temperatures induced by a lower thermal conductivity and a higher third cycle rating. It is interesting to separately quantify these two contributions and at the same time illustrate the transition from UO_2 to MOX type behaviour. For this demonstration a typical 3-cycle UO_2 case was selected from the ENIGMA database for comparison with rod 4567. The two power histories are compared in Fig. 11. The UO_2 rod burn-up was 40.1 MWd/kgHM and its measured release 0.65% with a corresponding ENIGMA prediction of 0.5%.

Fig. 12 shows how the predictions for this rod are affected by two changes: (a) conductivity reduced to 92% of normal; (b) 92% conductivity and ratings adjusted. The rating adjustment is a crude attempt to simulate the in-reactor operational strategy for MOX in a UO_2 core that results in higher third cycle power levels. Here, the rating has been reduced by 5% for all steps in the first half of its exposure, then increased by 5% for all steps in the second half. Obviously this method preserves the overall burn-up. With no changes, the peak temperatures fall well short of the threshold. The predicted releases are 0.50% average, 0.7% peak. With the 8% conductivity reduction the peak temperatures just graze the threshold. The predicted releases increase to 0.68%

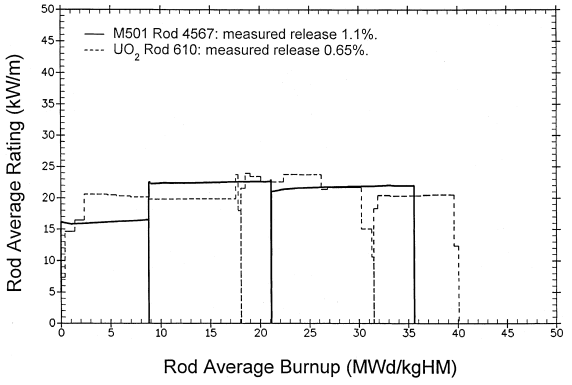

Fig. 11. Comparison of the rating history for SBR MOX rod 4567 with that for the UO_2 rod chosen for the illustration of the effects of thermal conductivity and third cycle power on gas release.

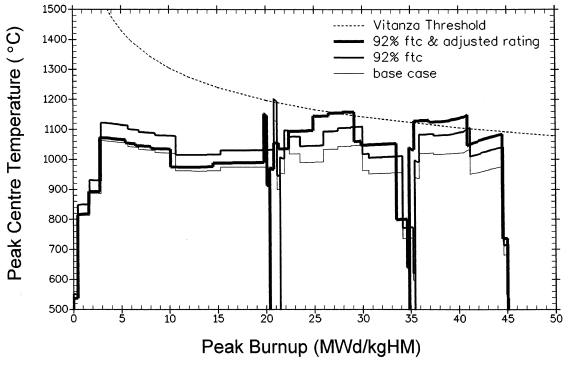

Fig. 12. Plot illustrating how the ENIGMA temperature and gas release predictions for the 'typical' UO_2 rod are affected by changes to thermal conductivity and rating. With no changes the peak temperatures fall well short of the threshold and the release is 0.5% average. With 8% conductivity reduction the peak temperature grazes the threshold and the release rises to 0.9% peak. When the rating is increased 5% in addition, the peak temperatures cross the threshold and the final release is 1.07% average, 1.8% peak. The rise in temperature with reduced conductivity (approx. 60°C) and rating increase (approx. 50°C) are notable.

average, 0.9% peak. When the ratings are adjusted on top of the conductivity reduction the peak temperatures cross the threshold and the release is increased to 1.07% average, 1.8% peak. These final values are very close to those for rod 4567.

Whilst these ENIGMA calculations, as a whole, are only intended for illustration, the peak rod temperatures reached are notable. Over the final 15 MWd/kgHM burn-up the increases in peak zone fuel centre temperature due to the 8% conductivity reduction and 5% rise in rating are, respectively, approximately 60°C and 50°C, giving a total temperature rise of about 110°C above the standard UO_2 figure.

8. Summary and conclusions

A detailed analysis of the fission gas release from seven SBR MOX rods irradiated in Beznau-1 to burn-ups of around 33 MWd/kgHM has been presented in this paper. The study included the measurement of rod internal pressure, rod free volume and the isotopic composition of the released gases. In all cases the rod internal volume decreased by about 35% during the irradiation, principally as a result of clad creep-down. A key feature of the calculation of fission gas release was the use of the physics code CASMO to obtain an accurate lifetime fission mix for the M501 rods together with a value for the ^{135}Xe to ^{136}Xe conversion ratio, α. These parameters are required for the determination of the individual isotopic and, therefore, overall fission gas yields. The values of the release fractions ranged from 0.4% to 1.1%. Correlation with calculated peak centre temperatures using the ENIGMA code showed that the fission gas release threshold for SBR MOX fuel is similar to that for standard UO_2 fuel. This suggests that the mechanisms responsible for the onset of fission gas release in this homogeneous fuel are similar to those in UO_2. It was further demonstrated, through extended use of ENIGMA, that any differences between the two fuel types, at least in the early stages of gas release, arise from the higher temperature experienced by MOX. This is a consequence of its lower thermal conductivity and the higher ratings generally experienced in its final cycle. Comparison with fission gas release data for MIMAS-AUC MOX, with a burn-up in the range 30–35 MWd/kgHM, showed that whilst the levels of release were similar the SBR fuel had slightly higher ratings in the third and final cycle. Overall, the performance of SBR MOX at burn-ups in the range 31–36 MWd/kgU is similar to that of the more homogeneous French fuels, COCA and MIMAS-ADU.

Acknowledgements

The authors gratefully acknowledge the contributions of Andy Worrall and Philip Keates of BNFL, Springfields, who performed the CASMO code calculations.

References

[1] P.M.A. Cook, I.D. Palmer, R. Stratton, C.T. Walker, in: IAEA International Symposium on MOX Fuel Cycle

Technologies for Medium and Long-Term Deployment, Vienna, Austria, 1999, Paper No. IAEA-SM-358-16.
[2] C. Brown, P.M.A. Cook, J. Edwards, S.B. Fisher, G.A. Gates, I.D. Palmer, R.J. White, in: Proceedings on TopFuel'99: LWR Nuclear Fuel Highlights at the Beginning of the Third Millennium, Avignon, France, SFEN, Paris, 1999, p. 223.
[3] J.A. Turnbull, J. Nucl. Mater. 38 (1971) 203.
[4] J.A. Turnbull, Radiat. Eff. 53 (1980) 243.
[5] C. Vitanza, E. Kolstad, V. Graziani, in: Proceedings of ANS Topical Meeting on LWR Fuel Performance, Portland, OR, USA, ANS, La Grange Park, IL, 1979, p. 366.
[6] R. Hargreaves, D.A. Collins, J. Brit. Energy Soc. 15 (1976) 311.
[7] R.J. White, M.O. Tucker, J. Nucl. Mater. 118 (1983) 1.
[8] W. Goll, H.P. Fuchs, R. Manzel, F. Schlemmer, Nucl. Technol. 102 (1993) 29.
[9] P. Deramaix, D. Haas, J. van de Velde, Nucl. Technol. 102 (1993) 47.
[10] Y. Guerin, J. Noirot, D. Lespiaux, C. Stuzick, P. Garcia, P. Blanpain, G. Chaigne, in: ANS Internationl Topical Meeting on LWR Fuel Performance, Park City, UT, USA, ANS, La Grange Park, IL, 2000, p. 706.
[11] R. Eastman, S. Tod, in: IAEA International Symposium on MOX Fuel Cycle Technologies for Medium and Long-Term Deployment, Vienna, Austria, 1999, Paper No. IAEA-SM-358-9.
[12] P. Garcia, A. Boulore, Y. Guerin, M. Trotobas, P. Goeriot, in: ANS International Topical Meeting on LWR Fuel Performance, Park City, UT, USA, ANS, La Grange Park, IL, 2000, p. 679.
[13] P. Ivison, S.B. Fisher, in: Proceedings on TopFuel'99: LWR Nuclear Fuel Highlights at the Beginning of the Third Millennium, Avignon, France, SFEN, Paris, 1999, p. 504.
[14] P. Ivison, P.M.A. Cook, S. Bremier, C.T. Walker, in: IAEA TCM on Water Reactor Fuel Element Modelling at High Burnup and Experimental Support, Windermere, England, 19–23 June 2000, Paper No. 4.2.
[15] P. Cook, R. Stratton, C.T. Walker, in: ANS International Topical Meeting on LWR Fuel Performance, Park City, UT, USA, ANS, La Grange Park, IL, 2000.
[16] C.T. Walker, W. Goll, T. Matsumura, J. Nucl. Mater. 228 (1996) 8.
[17] JEF-PC: A Personal Computer Program for Displaying Nuclear Data from the Joint Evaluation File Library, Version 1, IAEA/OECD, 1994.
[18] M. Edenius, D. Knott, K.S. Smith, in: International Conference on the Physics of Nuclear Science and Technology, Long Island, NJ, USA, October 1998, vol.1, p. 135.
[19] P. Blanpain, X. Thibault, M. Trotabas, in: ANS Topical Meeting on LWR Fuel Performance, West Palm Beach, FL, USA, ANS, La Grange Park, IL, 1994, p. 718.
[20] P. Blanpain, X. Thibault, J.P. Pagès, in: ANS Topical Meeting on LWR Fuel Performance, Portland, OR, USA, ANS, La Grange Park, IL, 1997.
[21] L. Brunel, P. Blainpan, G. Chaigne, M. Trotobas, in: IAEA International Symposium on MOX Fuel Cycle Technologies for Medium and Long-Term Deployment, Vienna, Austria, 1999, Paper No. IAEA-SM-358-14.
[22] I.D. Palmer, R.J. White, G. Rossiter, in: IAEA International Symposium on MOX Fuel Cycle Technologies for Medium and Long-Term Deployment, Vienna, Austria, 1999, Paper No. IAEA-SM-358-20.
[23] D. Sheppard, C. Vitanza, OECD Halden Project, Norway, Report HPR 229, August 1979.
[24] K. Joon, OECD Halden Project, Norway, Report HPR 211, 1977.
[25] R.O. Meyer, C.E. Beyer, J.C. Voglewede, Report NUREG-0418, 1978.
[26] R.B. Bellamy, J.B. Rich, J. Nucl. Mater. 33 (1969) 64.
[27] M.G. Balfour, Westinghouse Atomic Power, Report WCAP-3850-5, 1970.
[28] M. Conte, N. Vignesoult, in: IAEA Specialists Meeting on Internal Fuel Rod Chemistry, Erlangen, Fed Rep. Germany, 1979, IWGFPT/3, p. 95.